J|A|C|S ARTICLES

Published on Web 02/03/2009

Measuring and Relating the Electronic Structures of Nonmodel Supported Catalytic Materials to Their Performance

Eranda Nikolla, Johannes Schwank, and Suljo Linic*

Department of Chemical Engineering, University of Michigan, Ann Arbor, Michigan 48109-2136

Received November 27, 2008; E-mail: linic@umich.edu

Abstract: Identifying structure−performance relationships is critical for the discovery and optimization of heterogeneous catalysts. Recent theoretical contributions have led to the development of d-band theory, which relates the calculated electronic structure of a metal to its chemical and catalytic activity. While there are many contributions where quantum-chemical calculations have been utilized to validate the d-band theory, experimental examples relating the electronic structures of commercially relevant nonmodel catalysts to their performance are lacking. We show that even small changes in the near-Fermi-level electronic structures of nonmodel supported catalysts, induced by the formation of surface alloys, can be measured and related to the chemical and catalytic performance of these materials. We demonstrate that critical shifts in the d-band center in alloys are related to the formation of new electronic states in response to alloying rather than to charge redistribution among constitutive alloy elements, i.e., the number of d holes and d electrons localized on the constitutive alloy elements is constant. On the basis of the presented results, we provide a simple, physically transparent framework for predicting shifts in the d-band center in response to alloying and relating these shifts to the chemical characteristics of the alloys.

Introduction

It has been a long-standing goal of fundamental research in heterogeneous catalysis to establish universal relationships between the electronic and geometric structures of catalytic materials and their chemical and catalytic performance.[1−4] The recent theoretical work of Nørskov and co-workers[5−9] has led to the development of the d-band theory, which relates the electronic structure of a metal to its chemical activity and catalytic performance. In its simplest form, the d-band theory states that for a given geometry of an adsorbate on a surface adsorption site, the adsorption energy of the adsorbate depends on the position of the center of mass of the d electrons and d holes (the d-band center) of the atoms that form the adsorption site. In general, metals with the d-band center closer to the Fermi level are more chemically active than those with the d-band center further away from the Fermi level. The ultimate value of the d-band theory is that it represents a physically transparent framework for predictive heterogeneous catalysis, i.e., it allows us to relate even small changes in the electronic structure of an adsorption site (due to alloying, the formation of overlayers of one metal on another metal, chemical poisoning and promotion, etc.) to the chemical and catalytic properties of the site.[4−8,10−13] There are a few contributions where quantum-chemical density functional theory (DFT) calculations on model systems have been utilized to validate the d-band theory.[11,14−16] The experimental examples relating the electronic fingerprints of catalytic materials to their performance have been limited to two recent studies on well-defined model systems.[10,14] The studies of commercially relevant supported catalytic materials are lacking.

In this contribution, we have utilized a combination of scanning transmission electron microscopy (STEM) techniques and Auger electron spectroscopy (AES) to probe the near-Fermi-level surface electronic structure of nonmodel supported catalytic materials. We show that even small changes in the electronic structures of supported catalysts, induced by the formation of surface alloys, can be measured and related, in accordance with the d-band model, to the chemical activities and catalytic performance of these materials. We demonstrate that critical shifts in the d-band center in alloys are related to the formation of new electronic states in response to alloying and that the measured charge (the band filling below and above Fermi level) localized on the constitutive elements of the alloy is preserved. These observations allow us to propose a simple and physically

(1) Feibelman, P. J.; Hamann, D. R. *Phys. Rev. Lett.* **1984**, *52*, 61.
(2) Falicov, L. M.; Somorjai, G. a. *Proc. Natl.l Acad. Sci. U.S.A.* **1985**, *82*, 2207.
(3) Cohen, M. H.; Gandugliapirovano, M. V.; Kudrnovsky, J. *Phys. Rev. Lett.* **1994**, *72*, 3222.
(4) Harris, J.; Andersson, S. *Phys. Rev. Lett.* **1985**, *55*, 1583.
(5) Hammer, B.; Norskov, J. K. *Surf. Sci.* **1995**, *343*, 211.
(6) Hammer, B.; Morikawa, Y.; Norskov, J. K. *Phys. Rev. Lett.* **1996**, *76*, 2141.
(7) Hammer, B.; Norskov, J. K. *Nature* **1995**, *376*, 238.
(8) Norskov, J. K.; Bligaard, T.; Logadottir, A.; Bahn, S.; Hansen, L. B.; Bollinger, M.; Bengaard, H.; Hammer, B.; Sljivancanin, Z.; Mavrikakis, M.; Xu, Y.; Dahl, S.; Jacobsen, C. J. H. *J. Catal.* **2002**, *209*, 275.
(9) Hammer, B. *Top. Catal.* **2006**, *37*, 3.
(10) Nilsson, A.; Pettersson, L. G. M.; Hammer, B.; Bligaard, T.; Christensen, C. H.; Norskov, J. K. *Catal. Lett.* **2005**, *100*, 111.
(11) Greeley, J.; Mavrikakis, M. *Nat. Mater.* **2004**, *3*, 810.
(12) Delbecq, F.; Sautet, P. *Phys. Rev. B* **1999**, *59*, 5142.
(13) Pedersen, M. O.; Helveg, S.; Ruban, A.; Stensgaard, I.; Laegsgaard, E.; Norskov, J. K.; Besenbacher, F. *Surf. Sci.* **1999**, *426*, 395.
(14) Stamenkovic, V. R.; Mun, B. S.; Arenz, M.; Mayrhofer, K. J. J.; Lucas, C. A.; Wang, G. F.; Ross, P. N.; Markovic, N. M. *Nat. Mater.* **2007**, *6*, 241.
(15) Zhang, J. L.; Vukmirovic, M. B.; Xu, Y.; Mavrikakis, M.; Adzic, R. R. *Angew. Chem., Int. Ed.* **2005**, *44*, 2132.
(16) Xu, Y.; Ruban, A. V.; Mavrikakis, M. *J. Am. Chem. Soc.* **2004**, *126*, 4717.

10.1021/ja809291e CCC: $40.75

transparent model for predicting the shifts in the d-band center in response to alloying.

We present our findings in an example where the electronic structures of monometallic Ni and Sn/Ni alloy catalysts supported on yttria stabilized zirconia (YSZ) were measured and related to the chemical behavior of the catalysts. The Sn/Ni alloy contained ~2 wt % Sn with respect to Ni. Similar measurements were performed on Au/Ni and Ag/Ni catalysts (some of these are shown in the Supporting Information). The main conclusions for all three catalysts (Sn/Ni, Ag/Ni, and Au/Ni) were identical to each other. We have previously characterized the alloy catalyst, showing that Sn preferentially segregates in the surface layer of the Ni host, forming the Sn/Ni surface alloy.[17−19]

Experimental Methodology

Catalyst Synthesis. The Ni and Sn/Ni catalysts were supported on 8 mol % YSZ, which was prepared via a standard coprecipitation method. A mixture of yttrium nitrate [$Y(NO_3)_3 \cdot 6H_2O$] and zirconyl chloride ($ZrOCl_2 \cdot 2H_2O$) in deionized water was precipitated using a solution of ammonium hydroxide. After filtration, the precipitate was dried overnight and then calcined at 1073 K for 2 h. Ni was introduced onto the YSZ support by impregnation of nickel nitrate via the incipient wetness technique. The Ni loading in YSZ was ~15 wt % with respect to the total catalyst. After impregnation, the catalyst was calcined at 600 °C for 2 h in air in order to convert the nickel nitrate to nickel oxide. The catalyst was then reduced at 1173 K for 3 h using 30% H_2/N_2 to ensure full reducibility. The Sn/Ni/YSZ catalyst was synthesized by impregnating tin chloride ($SnCl_2 \cdot 4H_2O$) onto the NiO/YSZ catalyst via the incipient wetness technique. The nominal Sn loading was ~2 wt % with respect to the Ni content in the catalyst. The Sn/Ni/YSZ catalyst was also reduced at 1173 K for 3 h using 30% H_2/N_2.

EELS Experiments in the Scanning Transmission Electron Microscope. The electron energy loss spectroscopy (EELS) experiments were carried out in a JEOL 2010F field-emission electron microscope. The instrument was operated at 200 kV under a pressure of 1.5×10^{-7} Torr in scanning transmission electron mode. A Gatan imaging filter was utilized to collect the low-angle inelastically scattered electrons in order to obtain the EELS spectra, which were were analyzed using Digital Micrograph. The lens conditions during operation were defined for a probe size of ~0.2 nm, with a convergence angle of 13 mrad and a collection angle of 40 mrad. The energy resolution of the energy-loss spectra (defined by the full width at half-maximum of the zero-loss peak) was 1.4 eV at a dispersion of 0.3 eV per pixel.

The specimens for the electron microscopy experiments were prepared by directly placing the prereduced catalyst powders on holey carbon-coated copper grids. Once inside the electron microscope, the samples were heated under vacuum to 773 K to desorb any impurities. The size of the particles was measured using a number of techniques, including the analysis of X-ray diffraction spectra, Brunauer−Emmett−Teller (BET) surface area measurements, and TEM. The diameter of the analyzed particles was ~20 nm.

The electron energy-loss near-edge structure (ELNES) spectra were normalized with respect to the atomic cross section, which was calculated by integrating the area under the energy-loss spectra between 30 and 40 eV above the onset of the Ni L_3 edge.[20,23] The background effects were subtracted using a standard power-law method.[35]

XPS Experiments. X-ray photoelectron spectroscopy (XPS) experiments were conducted using a Kratos Axis Ultra XPS system with a 150 W Al (mono) X-ray gun. This instrument was operated under a pressure of 5×10^{-9} Torr. The samples were prereduced in a reaction chamber connected to the XPS system to avoid oxidation of the samples. The runs were conducted using a pass energy of 20 eV. A charge neutralizer was utilized to prevent sample charging. The instrument was calibrated with respect to the Au $4f_{7/2}$ line at 84 eV.

Reactor Studies. The kinetic studies were conducted isothermally in a packed-bed quartz reactor system. The diameter of the quartz reactor was 0.375 in. Approximately 0.01 g of Ni/YSZ or Sn/Ni/YSZ catalyst with a particle size of 150−200 μm was diluted in 0.5 g of quartz powder (250−400 μm) and loaded in the packed bed reactor. In each case, the catalyst was reduced at 1173 K under a stream of 30% H_2/N_2 for 3 h prior to measuring reaction rates. The rates of methane steam reforming were measured as the temperature was varied from 923 to 1073 K. The absence of diffusion and mass transport limitations was confirmed by analyzing the rates as the total space velocity changed. The setup included a set of mass-flow controllers, a pair of thermocouples (inside and outside the reactor), and syringe pumps for water delivery. The lines after the water inlet were heated to 473 K to avoid condensation. The reactor effluent was analyzed using a gas chromatograph (Varian CP 3800) equipped with thermal conductivity detectors and a flame ionization detector.

DFT Calculations. The Dacapo pseudopotentials plane wave code (http://www.camp.dtu.dk) was employed for all of the calculations. Our approach was to find a set of parameters that ensured the relative convergence, i.e., the convergence of the respective energies of various structures. For the Ni(111) model system, we utilized 3×3 supercells with four-layer slabs and 54 special Chadi−Cohen k-points. For the Sn/Ni(111) model system, $^1/_3$ of the Ni surface atoms were replaced by Sn in a striped structure. Six layers of vacuum separated the slabs, and a dipole-correction scheme was employed to electrostatically decouple the slabs. The GGA-PW91 functional was employed for self-consistent spin-polarized electronic structure calculations. Vanderbilt pseudopotentials were employed to describe the core electrons. The density of valence electrons was determined self-consistently by iterative diagonalization of the Kohn−Sham Hamiltonian using Pulay mixing of densities. The plane-wave basis set used to describe the one-electron states was cut off at 350 eV. An electronic temperature of 0.1 k_BT was utilized during calculations, with the final results extrapolated to 0 K. In the geometry optimization calculations on the (111) surface termination, the top two substrate layers and adsorbates were allowed to fully relax. The forces were minimized to 0.05 eV/Å.

The oscillator strength $F(E)$ (shown in Figure 3 in Electronic Structure Measurements, below) is the quantity that describes the strength of the transition from one electronic state to another, and it corresponds directly to the information obtained in the experimental ELNES measurements. $F(E)$ was calculated from first principles as[20,22]

$$F(E) = T(E) \times \mathrm{LDOS}(E) \tag{1}$$

where LDOS(E) is the local density of states projected on an atom (Ni in this case) at energy E and $T(E)$ is a transmission function, given by

$$T(E) = \frac{1}{3}\frac{2m}{\hbar^2}E\sum_{i,f}|\langle f|r|i\rangle|^2 \tag{2}$$

The transmission function describes the radial overlap between the initial state $|i\rangle$ and the final state $|f\rangle$.[20] It varies slowly with energy and gives the basic edge shape of the spectra. The transmission function for the Ni $L_{2,3}$ edge was calculated previously by Muller et al.[22] using linear augmented plane wave (LAPW) optical oscillator strengths and the LAPW-projected LDOS for Ni. Strictly

(17) Nikolla, E.; Holewinski, A.; Schwank, J.; Linic, S. *J. Am. Chem. Soc.* **2006**, *128*, 11354.
(18) Nikolla, E.; Schwank, J.; Linic, S. *J. Catal.* **2007**, *250*, 85.
(19) Nikolla, E.; Schwank, J.; Linic, S. *Catal. Today* **2008**, *136*, 243.
(20) Keast, V. J.; Scott, A. J.; Brydson, R.; Williams, D. B.; Bruley, J. *J. Microsc. (Oxford, U.K.)* **2001**, *203*, 135.

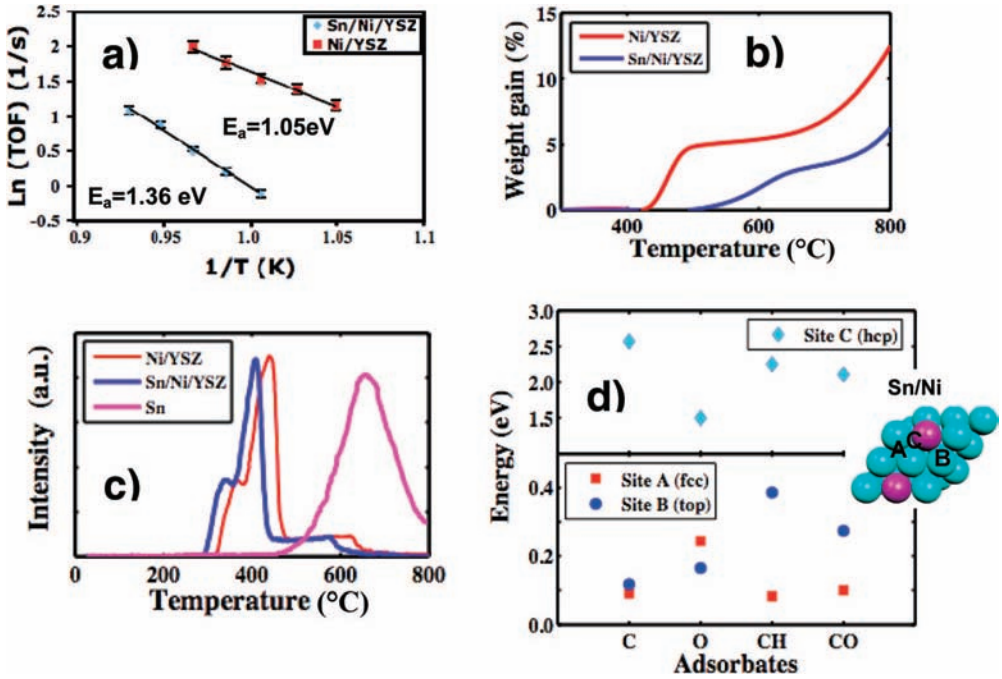

Figure 1. (a) Catalytic turnover frequency for steam reforming of methane on supported Ni and Sn/Ni alloy as a function of inverse temperature. The slopes of the lines are proportional to the corresponding overall activation barriers. (b) TGA studies of methane decomposition over supported Ni and Sn/Ni. (c) TPR measurements for Sn/Ni and monometallic Ni and Sn. (d) DFT-calculated energies for different adsorbates (O, C, and CH) at various sites on the Sn/Ni(111) alloy. The energy values for a particular site are referenced to the geometrically identical site on monometallic Ni(111).

speaking, while the transmission function is dependent on the local environment, this dependence is small. Therefore, in our calculations of oscillator strengths for the $L_{2,3}$ edges, we used the transmission function calculated for pure Ni. The LDOS for Ni surface atoms in Ni(111) and Sn/Ni(111) were calculated using the Dacapo plane-wave DFT code by projecting the plane waves onto spherical harmonics. The cutoff used in the calculations of the Ni d LDOS and the transmission function was 1.3 Å. The product of these two functions (i.e., the oscillator strength) is independent of the cutoff.

To calculate the broadened oscillator strength (i.e., the calculated ELNES), we utilized Lorentzian broadening for the lifetimes of the excitations by broadening the initial and final states, as described in refs 22 and 36. Gaussian broadening was applied to account for instrumental resolution. The broadening parameter was estimated on the basis of the instrument resolution, defined by the full width at half-maximum of the zero-loss peak.

Results

Chemical Measurements. In the discussion below, we first introduce the experimental measurements that allowed us to make a few general observations regarding the chemical activities of the nonmodel Ni and Sn/Ni catalysts. This is followed by an analysis of the relationships between the measured electronic structures of the materials and their chemical activities.

To study the chemical activities of the supported Ni and Sn/Ni catalysts, we performed a number of measurements aimed at quantifying adsorption, desorption, and activation of molecules on the catalysts. All of the measurements showed that the supported monometallic Ni catalyst is inherently more chemically active (interacts more strongly with adsorbates) than the Sn/Ni catalyst (Figure 1).[17−19] For example, an Arrhenius analysis of the steady-state reactor data obtained for steam reforming of methane (our kinetic isotope labeling studies and previous contributions of others demonstrated that the rate of methane steam reforming is controlled by the activation of C−H bonds in methane for both catalysts) showed that the overall activation barrier is ∼0.3 eV higher on supported Sn/Ni than on supported monometallic Ni for Sn/Ni and Ni particles having identical diameters (Figure 1a). Identical conclusions were obtained in thermal gravimetric analysis (TGA) experiments (Figure 1b). In these measurements, the catalyst was exposed to methane, and the catalyst's weight was measured as the temperature increased. As methane was activated, the weight of the catalyst increased as a result of the deposition of carbon on the catalyst. The measurements showed that the C−H bond is activated with an activation barrier that is ∼ 0.26 eV lower on supported Ni than on Sn/Ni. Similar conclusions regarding the relative chemical activities of Ni and Sn/Ni were obtained in various molecular desorption studies. For example, temperature programmed reduction (TPR) experiments showed that the reduction temperature for the Sn/Ni catalyst was lower than those for monometallic Ni and Sn substrates (Figure 1c). Quantitative analysis of the TPR data showed that the activation barrier for the oxygen reduction is ∼0.09 eV lower on Sn/Ni than on monometallic Ni. Using temperature programmed desorption (TPD) of molecular CO and atomic oxygen, we also measured the activation barriers for CO and O_2 desorption to be ∼0.1 eV lower on supported Sn/Ni than on Ni.

The difference in the chemical activities of pure Ni and the Sn/Ni alloy can be related to the Sn-induced changes in the geometric and electronic structure of Ni. For example, the difference in the C−H activation barriers on Sn/Ni and Ni can to a large degree be explained by a geometric effect where Sn blocks the low-coordinated Ni sites on Ni particles, which are efficient in the activation of C−H bonds. On the other hand, the smaller differences between Ni and Sn/Ni in the desorption of oxygen and CO, as measured in the TPR and TPD experiments, are mainly related to Sn-induced modifications in the electronic structure of the Ni atoms. The reason for this is that the O and CO adsorbates interact weakly with the Sn sites

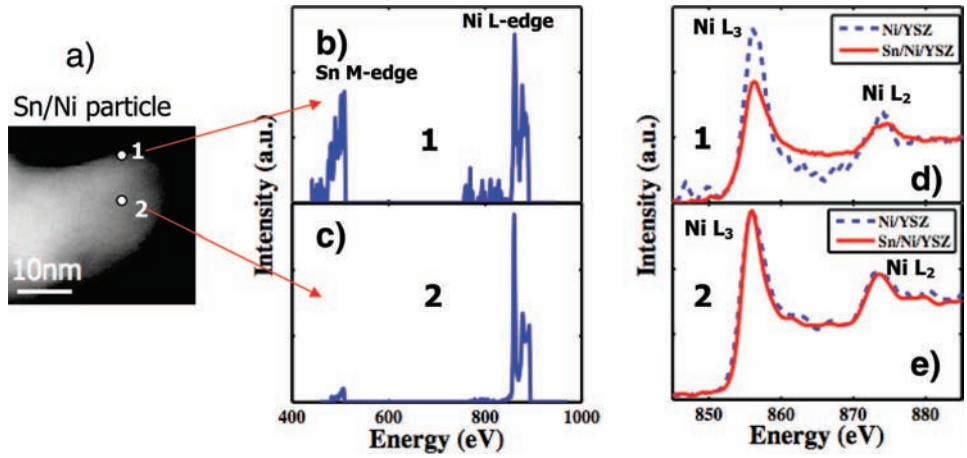

Figure 2. (a) STEM image of a Sn/Ni particle supported on YSZ. (b) EELS spectra obtained with a ~0.2 nm electron beam focused on the edge of the Sn/Ni particle (labeled as "1"). (c) EELS spectra with the electron beam focused on the center of the particle (labeled as "2"). (d) Ni $L_{2,3}$ ELNES for the surface regions of pure Ni and Sn/Ni. (e) Ni $L_{2,3}$ ELNES for the bulk regions of Ni and Sn/Ni.

of the Sn/Ni surface alloy, i.e., the adsorption of CO and O on Ni and Sn/Ni takes place only at the geometrically identical Ni sites on the two catalysts. This is illustrated in Figure 1d, where we have plotted the DFT-calculated adsorption energies for different adsorbates at various sites on Ni and Sn/Ni. Figure 1d shows that adsorbate binding energies for the adsorption sites where Sn interacts directly with the adsorbates (site C in Figure 1d) are significantly less exothermic than the adsorption energies on pure Ni. The figure also shows that for the geometrically identical Ni sites (sites A and B in Figure 1d), the DFT-calculated adsorption energies of oxygen, CO, carbon, and CH fragments are also less exothermic on Sn/Ni than on Ni, implying that the inherent chemical activity of the Ni atoms is affected by their electronic interaction with the Sn atoms. The agreement between the calculated Sn-induced changes in the adsorption energies for CO and oxygen and the measured changes in the activation barriers for the respective desorptions of CO and O_2 is reasonable. The small discrepancies between calculated and measured energies are probably due to adsorbate-coverage effects and the accuracy of DFT. We note that the Sn-induced decrease in the adsorption energies of C and CH fragments at the Ni sites of Sn/Ni has significant practical implications, since it results in lower concentrations of the carbon-containing species on Sn/Ni during hydrocarbon reforming reactions, which ultimately improves the tolerance of these materials to carbon-induced deactivation.[17−19]

Electronic Structure Measurements. We performed a number of studies, including EELS and AES measurements, aimed at identifying the critical electronic features that drive the observed differences in the chemical activities of the geometrically identical sites on the Ni and Sn/Ni catalysts. We selected these techniques to study the surface electronic structure of the supported catalysts because they allowed us to independently probe the states slightly above (EELS) and below (AES) the Fermi level. This was necessary to draw rigorous conclusions about the filling of the d band below and above the Fermi level and the shifts in the d-band center. Furthermore, a focused electron beam offers high spatial resolution and surface sensitivity.

In EELS experiments, a high-energy electron beam (~0.2 nm in diameter) is transmitted through a specimen, exciting electrons from the core energy levels to local unoccupied states above the Fermi level. The process generates atom-specific signals (from electron energy loss) known as ionization edges. Ionization edges also have small intensity fluctuations that depend on the local chemical environment.[20] The intensity fluctuations just above the onset of the ionization edge (up to 30−40 eV above the onset) are called the electron energy-loss near-edge structure (ELNES) and can be related to the unoccupied electronic states above the Fermi level that are localized on the atom from which the core electron was excited.[20−27] For example, in the case of Ni, electrons can be ejected from the $2p_{1/2}$ and $2p_{3/2}$ core energy states into the unoccupied 3d states, generating the L_2 and L_3 edges, respectively.

Figure 2b,c shows the EELS spectra for supported Ni and Sn/Ni particles obtained with a scanning transmission electron microscope with the electron beam focused either on the region close to the boundary of a particle, probing mainly the electronic structure of the particle surface, or the region close to the center of the particle, probing mainly the particle bulk. Figure 2b,c shows that the ratio of the Sn M edge to the Ni L edge is the highest when the boundary of the Sn/Ni catalytic particle is probed, and it decreases as the electron beam is moved closer to the center of the particle. These observations are consistent with our previous studies showing that Sn preferentially segregates at the surface of the Sn/Ni particles. Figure 2d,e shows the measured Ni $L_{2,3}$ ELNES for the two regions of the Ni and Sn/Ni particles, normalized with respect to the atomic cross section (see Experimental Methodology). The figure shows that the Ni $L_{2,3}$ ELNES for regions close to the centers of the Ni and Sn/Ni particles are almost identical to each other (Figure 2e), which is not surprising in view of the fact that in both cases the spectra are dominated by Ni atoms in the bulk. On the other hand, when regions close to the boundaries of the catalytic particles are probed, the Ni $L_{2,3}$ ELNES for the Sn/Ni particle is broadened compared with that of the monometallic Ni particle (Figure 2d).

(21) Muller, D. A.; Mills, M. J. *Mater. Sci. Eng., A* **1999**, *260*, 12.
(22) Muller, D. A.; Singh, D. J.; Silcox, J. *Phys. Rev. B* **1998**, *57*, 8181.
(23) Botton, G. A.; Guo, G. Y.; Temmerman, W. M.; Humphreys, C. J. *Phys. Rev. B* **1996**, *54*, 1682.
(24) Pearson, D. H.; Ahn, C. C.; Fultz, B. *Phys. Rev. B* **1993**, *47*, 8471.
(25) Muller, D. A.; Batson, P. E.; Silcox, J. *Phys. Rev. B* **1998**, *58*, 11970.
(26) Muller, F.; de Masi, R.; Steiner, P.; Reinicke, D.; Stadtfeld, M.; Hufner, S. *Surf. Sci.* **2000**, *459*, 161.
(27) Potapov, P. L.; Kulkova, S. E.; Schryvers, D.; Verbeeck, J. *Phys. Rev. B* **2001**, 6418.

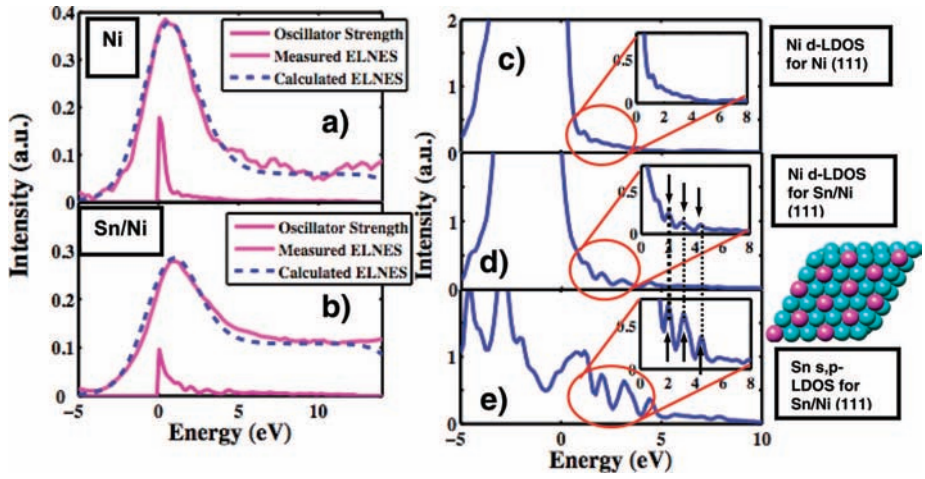

Figure 3. (a) Calculated Ni $L_{2,3}$ oscillator strength, calculated broadened Ni $L_{2,3}$ oscillator strength (calculated ELNES), and measured Ni $L_{2,3}$ ELNES for pure Ni. (b) Calculated Ni $L_{2,3}$ oscillator strength, calculated broadened Ni $L_{2,3}$ oscillator strength (calculated ELNES), and measured Ni $L_{2,3}$ ELNES for the Sn/Ni alloy. (c) Calculated local density of d states projected on a Ni surface atom in Ni(111). (d) Calculated local density of d states projected on a Ni surface atom in Sn/Ni(111). (e) Calculated local density of s and p states projected on a Sn surface atom in Sn/Ni(111). The arrows between the insets in (d) and (e) point to the hybridization between the d states of Ni and the s and p states of Sn. The Sn/Ni(111) surface alloy model system is shown in the inset at the right.

We find that the broadening of the Ni $L_{2,3}$ near edge for the Sn/Ni particles is associated with the formation of new electronic states above the Fermi level due to hybridization between the d states of Ni atoms and the s and p states of the neighboring Sn atoms. This is illustrated in Figure 3c−e, where the DFT-calculated LDOS projected on a Ni atom in the surface layers of monometallic Ni(111) (Figure 3c) and the Sn/Ni(111) surface alloy (Figure 3d) as well as the Sn LDOS for the Sn/Ni(111) surface alloy (Figure 3e) are shown. We performed calculations on the (111) surfaces, since they are the lowest-energy surfaces and describe the most dominant terrace sites on a catalytic particle. Thermodynamic simulations of Sn/Ni particles with relevant diameters (∼20−30 nm) and Sn concentration (∼2 wt % with respect to Ni), based on the Wulf−Kaishev formalism with surface energies for different Sn/Ni surface facets calculated using DFT,[28] showed that the Sn/Ni(111) surface structure, depicted in the inset at the right in Figure 3, dominates the surface of these Sn/Ni particles. To quantitatively relate the Ni LDOS to the measured ELNES, we calculated from first principles the oscillator strength $F(E)$ (this quantity is directly related to the measured ELNES signal) for the excitation of electrons from the localized Ni 2p states to the localized Ni 3d states in monometallic Ni(111) and the model Sn/Ni(111) surface (see Experimental Methodology).[20,22] Figure 3a,b shows that when we account for the finite lifetime of the excitations and the instrumental resolution (see Experimental Methodology), which broaden the calculated oscillator strength, the calculated spectra are almost identical to the measured Ni $L_{2,3}$ ELNES, thus reinforcing the notion that the formation of the Sn/Ni surface alloy results in broadening of the unoccupied Ni d states above the Fermi level due to hybridization between the Sn s and p states and the Ni d states and further supporting the model of the Sn/Ni particle surface.

(28) In these calculations, the energies of various Sn/Ni structures, including those where Sn displaces Ni from the bulk, subsurface, or surface, were calculated using DFT. The calculated energies were an input into thermodynamic simulations that allowed us to identify the lowest-energy structure of Sn/Ni particles following the Wulf−Kaishev theorem. For the relevant particle sizes and Sn concentrations of interest, the Sn/Ni particles were dominated by the (111) facets with the Sn and Ni distribution shown in Figure 4.

Table 1. Integrated and Normalized (with Respect to Ni Atomic Cross Section) Values of the Measured Ni $L_{2,3}$ ELNES and Calculated Oscillator Strengths for YSZ-Supported Monometallic Ni and Sn/Ni Alloy[a]

	Ni L edge		oscillator strength	
catalysts	integrated	normalized	integrated	normalized
Ni/YSZ	3.48 ± 0.07	1.000	0.256	1.000
Sn/Ni/YSZ	3.41 ± 0.07	0.98 ± 0.04	0.255	0.997

[a] The range of integration for the measured Ni $L_{2,3}$ ELNES was −5 to 35 eV from the onset of the Ni L_3 edge. It included the near-edge regions of both the Ni L_3 and L_2 edges. The range of integration for the calculated oscillator strength was 0 to 10 eV above the Fermi Level.

To quantify the number of d states localized on Ni atoms above the Fermi level (d holes), we integrated the Ni $L_{2,3}$ ELNES for the Sn/Ni alloy and for monometallic Ni (Table 1). Table 1 shows that the integrated Ni $L_{2,3}$ ELNES for Ni and Sn/Ni catalytic particles are very similar to each other, with a variation of ∼2%. These observations suggest that while the shape of the ELNES changes upon the formation of the Sn/Ni surface alloy, the number of d holes localized on Ni does not change.

To probe the electronic states below the Fermi level, we utilized AES. In the case of Ni, where the width of the d band is larger than the interaction between two holes created in the d band upon the emission of the Auger electron, the shape of the Auger spectra for the $L_3M_{4,5}M_{4,5}$ electronic transition is sensitive to the width of the Ni LDOS just below the Fermi level.[29,30] The AES spectra for the Ni $L_3M_{4,5}M_{4,5}$ electronic transition in the supported Ni and Sn/Ni catalysts are shown in Figure 4d. The figure shows that the Ni Auger spectrum for Sn/Ni is broadened compared with that for pure Ni, indicating that the Ni d band below the Fermi level is broader for Sn/Ni than for monometallic Ni. These observations are further supported by the DFT-calculated Ni and Sn LDOS for pure Ni and Sn/Ni (Figure 4a−c), where the hybridized Sn−Ni states below the Fermi level are observed in the Sn/Ni surface alloy.

(29) Bennett, P. A.; Fuggle, J. C.; Hillebrecht, F. U.; Lenselink, A.; Sawatzky, G. A. *Phys. Rev. B* **1983**, *27*, 2194.
(30) Diplas, S.; Lehrmann, J.; Jorgensen, S.; Valand, T.; Watts, J. F.; Tafto, J. *Surf. Interface Anal.* **2005**, *37*, 459.

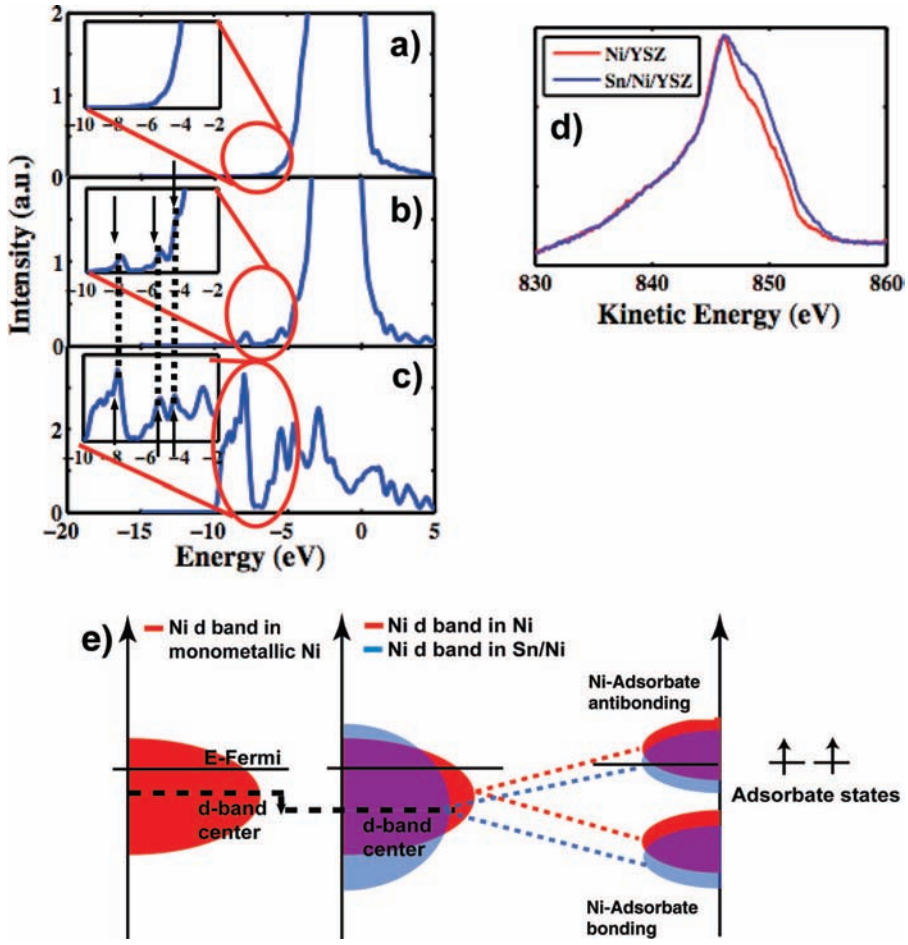

Figure 4. (a) Calculated local density of d states projected on a Ni surface atom in Ni(111). (b) Calculated local density of d states projected on a Ni surface atom in Sn/Ni(111). (c) Calculated local density of s and p states projected on a Sn surface atom in Sn/Ni(111). (d) Ni $L_3M_{4,5}M_{4,5}$ AES spectra for supported Ni and Sn/Ni. (e) Schematic illustration describing the interaction between a generic adsorbate and the Ni d bands in monometallic Ni and the Sn/Ni surface alloy.

Further quantitative analysis of the Auger spectra, including the evaluation of the ratio of the Ni $LM_{4,5}M_{4,5}$ and Ni $LM_{2,3}M_{4,5}$ intensities and ratio of the Ni $LM_{4,5}M_{4,5}$ Auger intensity to the Ni 2p XPS intensity for the Sn/Ni and pure Ni samples, showed that while the Ni d band below the Fermi level is broadened as a result of the Sn−Ni interaction, the number of states in the valence d band is preserved.

Discussion

ELNES and AES measurements suggest that the formation of the Sn/Ni surface alloy is accompanied by the formation of electronic states above and below the Fermi level. While these states broaden the Ni d band, they do not lead to a measurable charge transfer (electrons or holes) between Ni and Sn, i.e., the filling of the Ni d band below and above the Fermi level is identical for Ni atoms in monometallic Ni and Sn/Ni. We note that when we discuss charge transfer, we are referring to the change in the filling of electronic states localized on a particular atom, as measured by ELNES or as calculated from the oscillator strength spectra (i.e., this is not identical to various schemes for the division of charge, such as Bader or Mullikan). This definition of charge transfer is fairly universal, since it is independent of the cutoff radius over which the charge is integrated. To preserve the number of d holes and d electrons localized on Ni and in response to the formation of new states that broaden the d band, the center of the Ni d band in Sn/Ni must shift downward in energy with respect to that in monometallic Ni. This is illustrated in the schematic illustration in Figure 4e, which shows that as the d band gets broader, to preserve the number of states above and below the Fermi level (defined as the integral under the curve), the average energy of the d electronic states (the center of d band) shifts downward, away from the Fermi level.

The change in the electronic structure manifested in the downward shift in the d-band center has a number of consequences, including the diminished chemical activity of the geometrically identical Ni sites in Sn/Ni compared with monometallic Ni. This can be understood in terms of the d-band theory, as illustrated in the sketch in Figure 4e. For example, various adsorbates that are important in many catalytic processes, such as O, C, OH, CO, and CH_x fragments, interact with the d states of Ni via the formation of bonding and antibonding Ni−adsorbate states (orbitals). The position of the bonding and antibonding orbitals with respect to the Fermi level depends on the position of the substrate d-band center. For Ni atoms with the d-band center closer to the Fermi level (i.e., those in the monometallic Ni catalyst), the antibonding Ni−adsorbate states are higher in energy than the antibonding Ni−adsorbate states formed when the adsorbate interacts with Ni atoms in Sn/Ni. The consequence of this is that the antibonding adsorbate−Ni

states for Sn/Ni catalysts are populated to a higher degree than the antibonding states for monometallic Ni, which ultimately decreases the strength of interaction between the adsorbates (O, C, OH, CO, CH_x, etc.) and the Ni sites on the Sn/Ni substrate. These observations also suggest that the adsorbate/substrate interactions are not directly related to the number of d holes in the substrate.

The results of the studies presented here, which show that the interaction between Ni and Sn in the surface alloy is dominated by the formation of shared electronic states that are distributed in such a way that the filling of the Ni d band does not change (i.e., the numbers of d holes and d electrons are constant), contrast with various models arguing that the change in the electronic structure of constitutive elements in an alloy is due to the transfer of charge among the alloy elements.[31] Our results show that local potentials of constitutive metal elements and the screening process in metals minimize the charge transfer from one element to another. We have observed that the identical physical picture, where the changes in the position of the d-band center for various sites in alloys can be explained in terms of the preserved local charge and the formation of new electronic states which broaden the d band, explains the change in the electronic structure of the Ni sites in Ag/Ni and Au/Ni alloys (Figure S1 in the Supporting Information shows ELNES measurements for Au/Ni and Ag/Ni).[32] It is our hypothesis that identical observations regarding the constancy in the number of d holes and d electrons (i.e., constant filling of the d band below and above the Fermi level) in alloys and the shift in the electronic structure to accommodate this constancy can be made for almost any combination of two transition or noble metals that form bulk or surface alloys. One reason for this is that the constitutive elements in the alloys will have similar electronegativities [it has been observed empirically by Hume and Rothery (as expressed in the Hume−Rothery rules) that in order for two metallic compounds to form an alloy, they must have similar electronegativities], and the interaction between the elements will thus take place via the formation of hybridized electronic states. Another reason might be an innate tendency of metal atoms to maintain a constant local charge, as suggested in recent calculations by Raebiger et al.[34] We note that similar conclusions regarding the constancy of local charge on metals was also pointed out for Pt alloys on the basis of DFT calculations.[33]

Another critical consequence of the analysis presented here is that since the charge on constitutive alloy elements is preserved, the shift in the position of the d-band center in response to alloying, for a physically realistic shape of the d band (e.g., a realistic d band in metals can be approximated by a rectangle or parabola), is a function *only* of the width of the band. As shown in Figure 4e, if the d-band filling above and below the Fermi level is constant and the width changes, then the position of the center of the d band must change to preserve the number of states below and above the Fermi level. Since the change in the width of the d band in response to alloying is easily predictable, the shifts in the d-band center and therefore the changes in chemical activity induced by alloying in principle can also be predicted straightforwardly. The change in the width of the d band for a given geometry can be predicted on the basis of interatomic matrix elements (the spatial extent of the valence orbitals) that describe bonding between an atom and its environment (i.e., in this case, bonding between constitutive elements in alloys). The interatomic matrix elements are easily accessible and often tabulated in solid-state tables.[37] The relationship between the interatomic matrix elements of metals and the width of the d band was thoroughly discussed in recent DFT studies of adsorption on various alloys by Kitchin et al.,[33] who showed that for a given geometry, the width of the band is proportional to the spatial extent of the valence orbitals of the constitutive elements in the alloy. Since the spatial extents of the valence orbitals of Sn, Au, and Ag are larger than the spatial extent of the Ni orbitals, the formation of M/Ni alloys (M = Sn, Ag, Au) in which M atoms are substituted for Ni in the Ni matrix will lead to a broader Ni d band than in pure monometallic Ni, as was shown in our experiments. More importantly, since in general the spatial extent of the valence orbitals increases in going from right to left and from top to bottom among transition and noble metals in the periodic table, assuming that there is no charge transfer from one element in an alloy to another (as our results have shown) allows one to predict, for a given geometry, the direction of the shift in the center of the d bands of constitutive elements in different alloys and therefore the changes in the chemical activities of the alloys.

It is also important to briefly revisit the relationships between the electronic structure of a catalytic material and its performance. This relationship is critical for the development of systematic approaches for the discovery of new or improved solid-state heterogeneous catalysts. For example, the Sn-induced lowering of the center of the Ni d band (the decrease in the average energy of d electrons in the system) led us to conclude the following: (i) because of the lower electronic energy of this system compared with pure Ni, there should be a significant thermodynamic driving force to form the Sn/Ni surface alloy and sustain it under catalytic conditions; and (ii) the Sn/Ni catalyst binds carbon and carbon fragments less strongly than monometallic Ni, therefore decreasing the surface concentration of carbon-carrying intermediates on the catalyst surface during hydrocarbon reforming reactions and diminishing the driving force for the formation of solid carbon deposits, which are known to deactivate monometallic Ni catalysts. These physical characteristics of Sn/Ni are directly responsible for the experimentally established superior carbon tolerance of Sn/Ni compared with monometallic Ni in hydrocarbon reforming reactions.[17−19] A similar analysis would apply to Au/Ni and Ag/Ni alloys.

Conclusions

In conclusion, we have analyzed the changes in surface electronic structure associated with the formation of supported Ni alloy catalysts. We quantified the electronic states in the vicinity of the Fermi level using a number of experimental probes and showed that even small changes in the electronic structures of nonmodel supported catalysts, induced by the formation of surface alloys, can be related to the chemical

(31) Pollock, D. D. *Physical Properties of Materials for Engineers*, 2nd ed.; CRC Press: Boca Raton, FL, 1993.
(32) Besenbacher, F.; Chorkendorff, I.; Clausen, B. S.; Hammer, B.; Molenbroek, A. M.; Norskov, J. K.; Stensgaard, I. *Science* **1998**, *279*, 1913.
(33) Kitchin, J. R.; Norskov, J. K.; Barteau, M. A.; Chen, J. G. *Phys. Rev. Lett.* **2004**, 93.
(34) Raebiger, H.; Lany, S.; Zunger, A. *Nature* **2008**, *453*, 763.
(35) Egerton, R. F. *Electron Energy Loss Spectroscopy in the Electron Microscope*, 2nd ed.; Plenum Press: New York, 1996.
(36) Muller, J. E.; Wilkins, J. W. *Phys. Rev. B* **1984**, *29*, 4331.
(37) Harrison, W. A. *Electronic Structure and the Properties of Solids*; Dover Publications: New York, 1989.

activities and catalytic performance of these materials. These findings support models suggesting that the position of the center of the electronic d band can be related to the catalytic activity of the material. We have also found that the critical shifts in the d-band center in alloys are the result of the formation of new electronic states in response to alloying and that the electronic charge (the d-band filling below and above the Fermi level) on the constitutive alloy elements is preserved. These results provide a framework for predicting shifts in the d-band center in response to alloying. This framework is important for establishing universal structure−performance relationships that can guide us in the discovery of novel or improved heterogeneous catalysts.

Acknowledgment. We gratefully acknowledge the support of the U.S. Department of Energy, DOE-BES, Division of Chemical Sciences (FG-02-05ER15686), the NSF (CTS 0543067 and CBET 0756255), DOE-NETL (FC26-05-NT-42516), and the U.S. Army under Cooperative Agreement W56HZV-05-2-0001. We thank Dr. Kai Sun for his help with microscopy.

Supporting Information Available: ELNES spectra for Ag/Ni and Au/Ni alloys as well as the procedure used to synthesize the alloys. This material is available free of charge via the Internet at http://pubs.acs.org.

JA809291E